Modelling photovoltaic modules with neural networks using angle of incidence and clearness index

Michel Piliougine[1,*], David Elizondo[2], Llanos Mora-López[3] and Mariano Sidrach-de-Cardona[1]

[1]Departamento de Física Aplicada II, Universidad de Málaga, Louis Pasteur 35, 29071 Málaga, Spain
[2]DIGITS, Department of Computer Technology, De Montfort University, The Gateway, LE1 9BH Leicester, UK
[3]Dpto. de Lenguajes y Ciencias de la Computación, Universidad de Málaga, Louis Pasteur 35, 29071 Málaga, Spain

Abstract

A neural network for modelling photovoltaic modules using angle of incidence and clearness index is proposed. Engineers require methods to estimate the output of a photovoltaic plant depending on meteorological conditions. Therefore, models for the grid inverter and the generator must be provided and their outputs must be combined. The connection between both models is related to the maximum power point of the generator and how it is tracked by the inverter. That maximum power point under specific conditions of irradiance and module temperature is determined by the *I–V* curve of the module, which must be simulated under those conditions. Algebraic procedures were used to simulate the *I–V* curve. Recently, neural networks have been used for the same purpose. Previous methods only take into account the irradiance and the module temperature. The model proposed is based on neural networks and it uses not only the irradiance and the module temperature, but also the angle of incidence and the instantaneous clearness index as additional inputs. The normalised clearness replaces the standard clearness index since it allows the removal of the hourly trend found in this last index. This new model improves the results obtained with previous ones as it can distinguish amongst samples with the same solar irradiance and temperature values but with different angle of incidence and instantaneous clearness index. Results show that this model could be used to improve the accuracy of the tools used to forecast the output of photovoltaic plants.

1   Introduction

In order to design a photovoltaic power plant, it is necessary to provide an estimation of the power that the system will produce under different meteorological conditions. This can be done by modelling each component of the photovoltaic plant and combining their outputs. The performance of a grid inverter depends on its ability to track the maximum power point of the generator for variable irradiance and module temperature levels. This maximum power point must be determined by simulating the *I–V* curve under different conditions. Manufacturers provide the electrical parameters of photovoltaic modules at *standard test conditions* (STC). However, the information provided by the specifications is not enough to build an operational model valid for a wide range of irradiances and module temperatures. The tracking procedure is not only related to the absolute values of the electrical parameters, but also to the shape of the *I–V* curve.

Algebraic procedures can be found in the literature in order to determine the *I–V* curve of a PV module under different conditions of irradiance and cell temperature. These methods consist of a point-by-point extrapolation. A correction is applied to each current–voltage pair to translate it into a set of new conditions. The result is an approximation to the *I–V* curve that would be measured if the module were under the new conditions of irradiance and cell temperature. An example of algebraic method is the *procedure 1* of IEC 60891 standard [1]. The *I–V* curve for a given value of irradiance G and module temperature T can be simulated using a reference *I–V* curve measured under an irradiance G^* (1000 W/m^2) and a module temperature T^* (25 °C). It is only necessary to apply Eq. (1) and Eq. (2) to each point (V_i^*, I_i^*) of the reference curve (with $i = 1, \ldots, n$) in order to obtain the points $(\hat{V}_i, \hat{I}_i)$ of the simulated curve.

$$\hat{I}_i = I_i^* + I_{\text{SC}}^* \left(\frac{G}{G^*} - 1 \right) + \alpha(T - T^*) \tag{1}$$

$$\hat{V}_i = V_i^* - R_S(\hat{I}_i - I_i^*) - \kappa \, \hat{I}_i(T - T^*) + \beta(T - T^*) \tag{2}$$

In the above equations, I_{SC}^* is the short–circuit current of the reference curve and α, β, κ and R_S are the intrinsic parameters of the photovoltaic module. The values of these parameters can be calculated by means of additional procedures described in the IEC 60891 standard from experimental measurements. However, approximated values of these parameters are provided by the manufacturer. In the literature there are other algebraic methods which improve the method given by the standard [2–5].

An alternative approach is to use an artificial neural network (ANN) to create a model of a photovoltaic module. This approach is more flexible since the inputs considered for building the model can be easily modified. Several examples can be found in the literature where ANNs are used to generate *I–V* curves of photovoltaic modules [6–13]. In these works, ANNs are used in order to reconstruct the *I–V* curve of a module under given values of irradiance and module temperature.

The most important contribution of our paper is the introduction of the angle of incidence (AOI) and the normalised instantaneous clearness index as additional inputs to a multilayer perceptron neural network. The normalised instantaneous clearness index is a reformulation of the standard instantaneous clearness index which takes into account the air mass factor to normalise its value. It has been proved that the accuracy of the predicted curves improves when using these two additional inputs.

The rest of the paper is organised as follows: A review of the application of neural networks in order to simulate photovoltaic systems is presented in Section 2. The formulae used to estimate the angle of incidence and the clearness index are detailed in Section 3. The methodology proposed in this paper is described in Section 4, including the process followed for training the neural network. A discussion of the results is presented in Section 5. Finally, the conclusions of the paper are summarised in Section 6.

2 Neural networks applied to PV simulation

ANNs have been successfully applied to solve many real life applications, including the prediction of solar radiation and the modelling of photovoltaic systems. Kalogirou [14] presents a brief introduction to neural networks and a review of their application to solve typical energy problems.

Many authors have used neural networks to estimate and forecast the global solar radiation and the clearness index [15–19]. There are also some examples where this approach has been used as a tool to track the maximum power point of a PV generator, see for instance [20, 21].

Using a neural network as a model of a specific photovoltaic module it is possible to reproduce its characteristic curve at a given value of irradiance and cell temperature. Once the network has been trained, the I–V curve under new conditions can be calculated by providing the corresponding values for both irradiance and cell temperature as inputs.

Karatepe et al. [6] use a multilayer perceptron taking as inputs the values of irradiance and cell temperature and giving as output the parameters required by the single diode equivalent circuit. Then, these values used in the model to estimate more points of the I–V curve.

Di Piazza et al. [7] use a growing neural gas network to determine three points of the I–V curve: the short–circuit current I_{SC}, the open–circuit voltage V_{OC} and the maximum power point P_M (given by V_M and I_M). Then, these values are used to determine the parameters of the double–diode model. Eventually, the complete I–V curve is generated.

In a similar way, in the work by Dolan et al. [8], a multilayer perceptron is used to estimate five points of the curve (in addition to I_{SC}, V_{OC} and P_M, two other intermediate points are considered). These points are used to reconstruct the entire I–V curve of the module using its electrical model. They do not only take into account the electrical model of the module, but also the heat transfer with the environment and the influence of the shades and wind.

Almonacid et al. [9] study the electrical characterisation of mono–crystalline and poly–crystalline silicon modules using multilayer perceptrons. In other work, the same technique is used to the electrical characterisation of CIGS modules [10].

Zárate et al. [11] use an additional fictitious input, which represents the voltage coordinate for each point of the I–V curve. The output of the network is a unique neuron which provides the current value of each point.

Bonanno et al. [12] investigate the use of radial basis function neural networks in order to predict the I–V curve taking into account the irradiance and module temperature, applying this method to different technologies and for indoor and outdoor characterisation.

In these previous works based on neural networks only the irradiance and the module temperature are used as inputs to the model. However, there are measurements under the same irradiance and module temperature with different I–V curves because there are other external parameters which influence the module's behaviour. In our previous work [13], solar spectral information was included as an additional input to a multilayer perceptron, performing previous results. Nevertheless spectral measurements are hardly available in most cases. The main contribution of this paper is the inclusion of the AOI and the clearness index as additional inputs to the multilayer perceptron. This way we are providing to the model more information related to incident radiation. Both new inputs can be calculated in an easy way and with minimum computational effort.

Another novelty of this paper is the way of estimating the error between a measured curve and a simulated one. Previous works take into account the differences between each individual I–V point of one curve and its matching point of the other curve and then a mean squared root is applied. The problem with this approach is that, given two different curves, the estimated error depends on the position and distribution of the I–V points along the curves. However, we assume that the error between two curves is the enclosed area between them. Therefore, we provide a definition of the error between two curves independent of the exact position of the points of those curves.
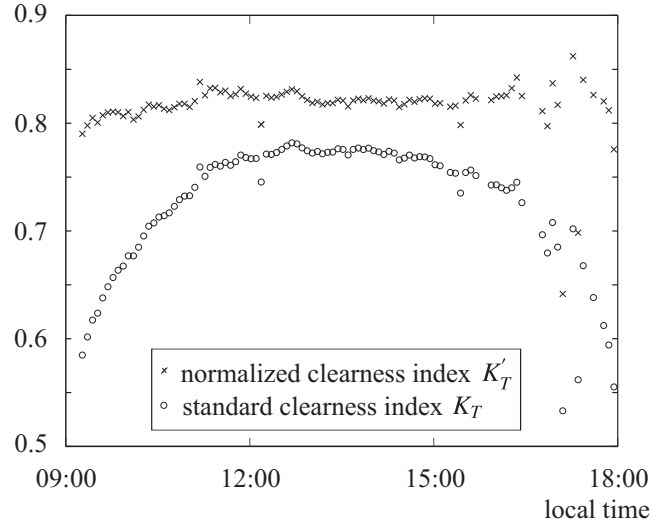
Figure 1: Angle of incidence as a function of the solar angles.

3   Calculation of additional inputs

In this section the formulae for the computation of the angle of incidence and the clearness index are detailed. This includes the necessary intermediate calculations. Both magnitudes will be used as additional inputs to the neural network in order to improve its performance.

3.1   Angle of incidence

In order to calculate the angle of incidence (AOI), it is necessary to determine the solar position at each time. An algorithm published by Reda and Andreas [22] was used to calculate three values: the Sun's topocentric elevation angle e (or its complementary, the zenith angle θ), the topocentric azimuth angle Γ and the Sun–Earth distance R (the term topocentric means that these measurements are taken from an observer on the Earth surface instead as opposed to one at the centre of the Earth). The inputs of the algorithm are the geographical coordinates (latitude, longitude and altitude) and the Ephemeris Julian Day (a unique value to express date and time in a linear scale used in Astronomy). The angle of incidence for an arbitrarily oriented module can be calculated based on its slope ω (measured from ground) and its rotation γ (from the South) using Eq. (3) (see Fig. 1):

$$\cos(\text{AOI}) = \cos\theta\cos\omega + \sin\theta\sin\omega\cos(\Gamma - \gamma) \tag{3}$$

3.2   Extraterrestrial irradiance

The beam extraterrestrial irradiance $G_{ext,b}$ (W/m^2) is defined as the irradiance at normal incidence outside Earth's atmosphere. The solar constant S_0 is the value of this magnitude at the mean Sun–Earth distance ($R_0 = 1$ AU $= 1.496 \times 10^8$ km). A good estimation of this value is 1366.1 W/m^2 [23]. The beam extraterrestrial irradiance when the Sun–Earth distance R differs from 1 AU can be calculated taking into account the inverse square law:

Figure 2: K_T and K_T' as a function of the local time on 23 February 2011.

$$G_{ext,b} = S_0 \cdot \left(\frac{R_0}{R} \right)^2 \tag{4}$$

In general, for an arbitrary orientation normal incidence does not occur. Therefore, we must estimate the incident extraterrestrial irradiance G_{ext} by reducing $G_{ext,b}$ using a factor equal to the cosine of the angle of incidence:

$$G_{ext} = G_{ext,b} \cdot \cos(\text{AOI}) \tag{5}$$

3.3 Air mass factor

The air mass factor quantifies the length of trail of the Sun's beams in the atmosphere. It is defined as the optical path length of the light when the Sun is at a given elevation divided by this value when the Sun is at the zenith. The air mass could be approximated using the formula given by Kasten and Young [24] as a function of the elevation angle:

$$\text{AM} = \frac{1}{\sin e + 0.50572 \cdot (e + 6.07995)^{-1.6364}} \tag{6}$$

The value of the air mass factor given above can be corrected using the atmospheric pressure value [25]:

$$\text{AM}_{\text{PC}} = \text{AM} \cdot \frac{P}{P_0} \tag{7}$$

where P is the measured pressure and P_0 is the standard atmospheric pressure at sea level (1013 mbar).

3.4 Instantaneous clearness index

Woyte et al. [26] define the instantaneous clearness index K_T on a arbitrarily oriented surface as the ratio between the measured global irradiance and the estimated extraterrestrial irradiance at the same orientation:

5

Geographical coordinates	
Longitude	4.48°W
Latitude	36.72°N
Elevation	50 m
PV module orientation	
PV module slope (from horizontal)	21°
PV module rotation (from south)	4°E

Table 1: Parameter values used for solar position calculations.

$$K_T = \frac{G}{G_{ext}} = \frac{G}{S_0 (R_0/R)^2 \cos(\text{AOI})} \qquad (8)$$

This index K_T depends on the zenith angle and consequently on the time of the day (see Fig. 2). However, an alternative formulation of the clearness index is proposed by Pérez et al. [27] to avoid that dependence. This new index is known as the normalised clearness index K_T' and it is defined as:

$$K_T' = \frac{K_T}{1.031 \cdot \exp\left(\frac{-1.4}{0.9 + \frac{9.4}{\text{AM}}}\right) + 0.1} \qquad (9)$$

where AM is the air mass calculated in Section 3.3 (instead of using AM we have taken AM_{PC}).

4 Methodology of application

In this work a multilayer perceptron was used to simulate the electrical behaviour of the photovoltaic module. A multilayer perceptron is a type of neural network made of an input layer, an output layer and one or several hidden layers (the number of hidden layers and units in each one are problem dependent and they need to be defined by the user beforehand). Each neuron of a layer is connected to all the neurons in the following layer. Each connection has an associated weight, which defines its strength, and must be adjusted during the training phase. The proposed model and its validation can be carried out following these steps:

4.1 Acquiring measured *I–V* curves

In this preliminary step several *I–V* curves are measured under different conditions of incident irradiance and module temperature.

Measurements were carried out on the roof of the photovoltaic laboratory at the University of Málaga in southern Spain. Table 1 gives the geographical coordinates of the laboratory and the orientation of the module used to build the model. The specifications of the module are also summarised in Table 2.

The typical meteorological conditions at the site of the installation are: 1,890 kWh/m^2 of annual global horizontal irradiation, average daytime air temperature of 18 °C, relative humidity of 63% and wind speed of 1 m/s. The set of measurements used in this work started on 1 February 2011 and finished on 22 May 2011. The interval of the measurement was set to 5 minutes.

The measurement system is based on a bipolar Kepco BOP (a four quadrant power supply). A computer controls the voltage sweep automatically whereas voltage and current of the module are measured using a pair of digital multimeters (current is sensed with the help of a shunt resistor). A

General features	
Dimensions (mm × mm × mm)	1208 × 654 × 39.5
Number of cells	66
Cells in series	33
Cells in parallel	2
Type of cell	mc–Si
Cell dimensions (mm × mm)	103 × 103
Cell area	104.4 cm^2
Electrical parameters at STC	
Short–circuit current I_{SC}	6.54 A
Open–circuit voltage V_{OC}	19.8 V
Maximum power P_M	94 W
Maximum power current I_M	5.88 A
Maximum power voltage V_M	16 V

Table 2: Main features of the photovoltaic module.

A	3152 samples with only G and T
A_1	100 samples randomly selected to train the ANN
A_2	3052 remaining samples to test the ANN
B	3152 samples with G, T, AOI and K'_T
B_1	100 samples randomly selected to train the ANN
B_2	3052 remaining samples to test the ANN

Table 3: Description of the training and testing sets.

waveform generator performs a square signal to trigger both multimeters simultaneously. The module temperature is measured through a RTD Pt100 sensor coupled to its back. The incident irradiance on the module surface is measured using a pyranometer. The control application allows us to measure *I–V* curves at regular intervals of time automatically. A complete description of the measurement system can be found in Piliougine et al. [28].

4.2 Selection of the training set

Due to the large volume of collected data, a subset of the *I–V* curves has been selected for the training process of the neural network model. We selected amongst all the measures in the database those that correspond to clear–sky days. We took into account only those days whose daily clearness index is over 0.7. Therefore, over the entire period of measurement, the following days were selected: 18, 23, 24, 25 and 28 February; 1, 2, 17, 18, 19, 24, 27, 30 and 31 March; 1, 7, 8, 9, 10, 12, 13, 14, 16, 26, 27 and 28 April; 5, 8, 9, 14, 21 and 22 May. In addition, only those records taken under an irradiance value greater than 200 W/m^2 were selected. In summary, a total of 3156 samples were used. Two initial data sets were created:

- A: 3156 *I–V* curves with values of G and T

- B: 3156 *I–V* curves with values of G, T, AOI and K'_T

A total of 100 samples were randomly selected to train the network and the remaining 3056 samples were used to test the models. Table 3 summarises these data sets. This selection procedure was performed for the sets A and B. Then, as can be seen in Table 3, there are 2 training sets (A_1 and B_1) and 2 testing sets (A_2 and B_2).

4.3 Preparing the training patterns

I–V curves are provided as tables of current–voltage pairs. The learning of a set of points is more complicated than the learning of a scalar parameter such as I_{SC} or V_{OC}, because it is necessary to find a format to represent *I–V* curves to be used in a neural network. In this work, a fictitious neuron is added to the input layer to represent the voltage coordinate of each point of the curve. In the output layer a single neuron represents the current associated to each voltage value.

The neural network has five inputs. The first four correspond to the meteorological conditions (G, T, AOI, K'_T), that must be fixed for each *I–V* curve. The last input is used to provide a varying voltage value in order to sweep different points of the same *I–V* curve. The output neuron will generate the corresponding current values.

Each table with voltage-current pair values must be transformed into a set of samples to train the network (as many as points belonging to the *I–V* curve). The sample corresponding to each *I–V* pair is made of the four fixed meteorological conditions and the varying value of voltage. The network is trained in order to generate the corresponding current value. In mathematical terms, we are mapping the initial function Ψ into another function Θ easier to manage with an MLP:

$$\Psi : \mathbb{R}^4 \rightarrow \mathbb{R}^{n \times 2} \qquad\qquad \Psi(G, T, \text{AOI}, K'_T) = \{(V_i, I_i)\}_{i=1}^n \quad (10)$$

$$\Theta : \mathbb{R}^5 \rightarrow \mathbb{R} \qquad\qquad \Theta(G, T, \text{AOI}, K'_T, V) = I \qquad\qquad (11)$$

4.4 Training of the multilayer perceptron

The Levenberg–Marquardt training algorithm was selected because it has a faster convergence than gradient descent [29]. There are several stop criteria to finish the training phase. The simplest is reaching the maximum number of iterations. Another possibility is achieving a gradient value lower than a minimum threshold. Validation check is another criterion to stop training and avoid over-fitting. Over-fitting occurs when the network learns the training set but presents difficulties generalising previously unseen patterns (testing set). Each time the network is trained, most of the samples are selected to adjust the weights, while the error of the few remaining samples is only monitored (validation error). When this error increases consecutively a certain number of times (fixed as a constant by the user), the network is starting to over-fit data and the training process must be stopped.

There is no rule to determine the number of hidden units in a MLP beforehand. We must experiment with different number of neurons performing multiple trainings and studying how this number affects the performance of the network. For this paper, the training process was repeated several times, starting from 2 hidden units up to 8 hidden units. Even with the same number of hidden units, each execution of the training algorithm is different, due to the random initialisation of the weights. Therefore, we must repeat the process a significant number of times (10 times in this experiment). In summary, we used 7 different topologies (varying from 2 to 8 hidden units) and each one was trained 10 times using MLP_{GT} (neural network with only G and T_m as inputs) and another 10 times using MLP_{ALL} (neural network with G, T_m, AOI and K'_T).

4.5 Generating *I–V* curves

On the one hand, there is a network MLP_{ALL} trained using G, T, AOI and K'_T. On the other hand, there is another network MLP_{GT} trained using only G and T. It is possible to simulate an *I–V* curve at given conditions (G, T, AOI, K'_T) following the scheme described in Fig. 3 (an analogous scheme could be used to generate a curve using MLP_{GT}). An array of voltage values $\hat{V}_i$ within a range is generated (this range must be fixed based on the electrical features of the module). Fixing the conditions of the measurement at the network input and varying the fictitious voltage input neuron (using the array
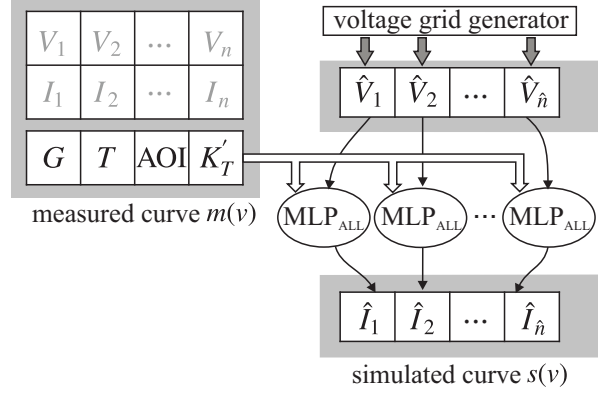
Figure 3: Scheme of the simulation of an I–V curve by a MLP.

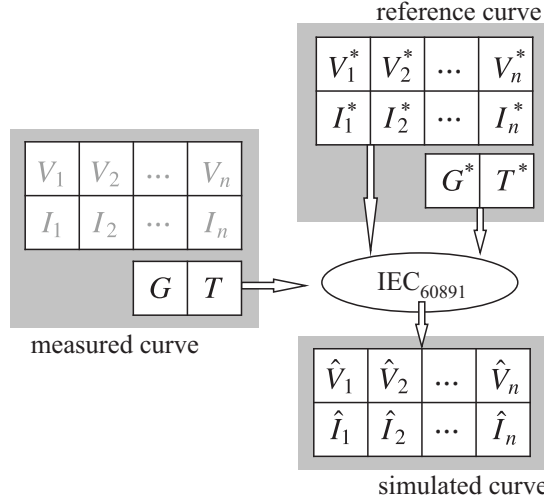Figure 4: Scheme of the simulation of an I–V curve by IEC 60891.

of voltage values), the network will return a sequence of current values $\hat{I}_i$ given by Eq. (12). The simulated curve is determined by the list of points $\{(\hat{V}_i, \hat{I}_i)\}$, where $i = 1, \ldots, \hat{n}$.

$$\hat{I}_i = \text{MLP}_{\text{ALL}}(G, T, \text{AOI}, K'_T, \hat{V}_i) \qquad i = 1, \ldots, \hat{n} \tag{12}$$

4.6   Validation of the model

In order to complete our study, a model based on the *procedure 1* of IEC 60891 was included (referred as IEC_{60981}). In order to apply the algebraic method (see Fig. 4), a reference I–V curve must be selected amongst all measured curves. For each sample of the testing set B_1, with its own value of irradiance and module temperature, the reference curve must be translated into those conditions using Eqs. (1) and (2).

The generalisation error of each model could be estimated using all the curves of the data set not seen during the training phase, i.e. the sets in Table 3 referred as A_2 and B_2. Each sample belonging to the testing set B_2 contains a measured curve $m(v) = \{(V_i, I_i)\}$ (where $i = 1, \ldots, n$) and its conditions of measurement, i.e., G, T, AOI and K'_T. For each model (MLP_{GT}, MLP_{ALL} or IEC_{60981}) and for each measured curve in the testing set, it is possible to generate a simulated curve $s(v) = \{(\hat{V}_i, \hat{I}_i)\}$ (where $i = 1, \ldots, \hat{n}$) and compare it with the measured curve $m(v)$ to estimate the error. In this work the error is estimated as the area enclosed between both curves within the first quadrant (see Fig. 5). If
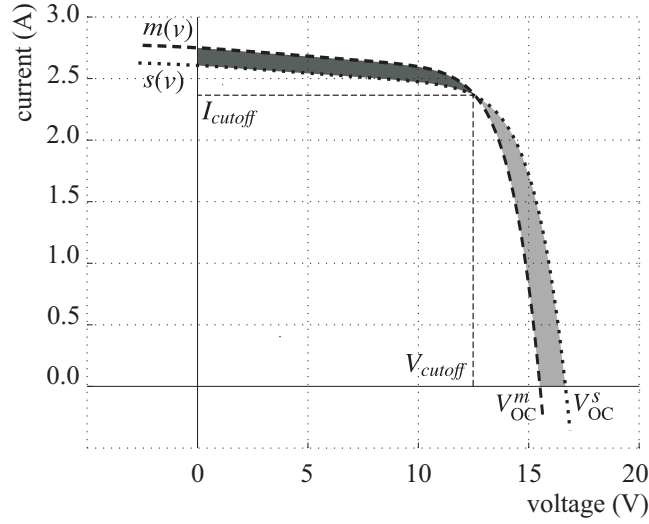
9

Figure 5: Estimation of the error between two I–V curves.

there were one or more cut-off points between both curves, this area must be calculated using different integration intervals. For example, two I–V curves $m(v)$ and $s(v)$ (measured curve and simulated one) with a unique cut–off point (V_{cutoff}, I_{cutoff}) are shown in Fig. 5. The error has one term measuring the enclosed area from $v = 0$ until V_{cutoff} and another term to quantify the enclosed area from V_{cutoff} until the end:

$$error = \left| \sum_{v=0}^{v \leq V_{cutoff}} m(v)\Delta v - \sum_{v=0}^{v \leq V_{cutoff}} s(v)\Delta v \right| + $$
$$+ \left| \sum_{V_{cutoff} \leq v}^{V_{OC}^m} m(v)\Delta v - \sum_{V_{cutoff} \leq v}^{V_{OC}^s} s(v)\Delta v \right| \tag{13}$$

As can be seen in Eq. (14), the relative error can be computed if the last value is divided by the area enclosed by the measured curve within the first quadrant. Finally, the global relative error of each method is calculated as the mean error amongst all the curves in the testing set.

$$relative\ error = \frac{error}{\left| \sum_{v=0}^{V_{OC}^m} m(v)\Delta v \right|} \tag{14}$$

4.7   Application of the model

The multilayer perceptron was trained using a filtered dataset composed of measurements taken under irradiance values over 200 W/m^2 and from clear–sky days (daily clearness index over 0.7). Hence, if the proposed method is to be of practical value, these criteria must be verified.

Although the model of the grid inverter is beyond the scope of this paper, the simulation of the photovoltaic plant requires an estimation of the I–V curve under changing conditions in time. In order to get different curves along the day, a forecasting of the evolution of the incident irradiance must be provided. Furthermore, using a thermal model of the module and the evolution of the other meteorological conditions (mainly air temperature and wind speed), the profile of cell temperature must be also estimated. The angle of incidence and the clearness index are calculated using the
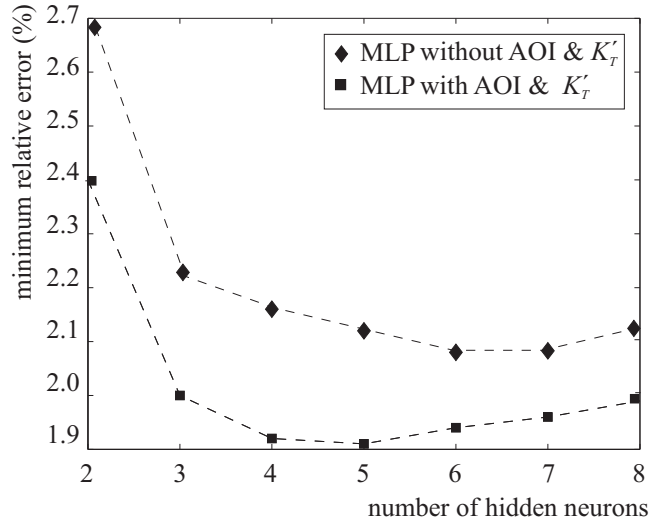
10

Figure 6: Relative error (%) as a function of the number of hidden units.

formulae described in section 3. Then, using MLP_{ALL} or MLP_{GT}, the *I–V* curves along a specific day can be predicted . Once we have obtained these curves, the inverter model is fed with this information, and the output of the plant along that day can be estimated.

5   Comparative results

In Fig. 6, for both the MLP_{GT} and the MLP_{ALL}, we have plotted the minimum value of the global relative error amongst the 10 repetitions of the same configuration as a function of the number of hidden units ($h = 2, \ldots, 8$). The introduction of the AOI and the normalised clearness index into the training process of the multilayer perceptron improves the global generalisation performance of the network. As we can see in Fig. 6, the best result for the MLP_{ALL} was achieved with 5 neurons in the hidden layer.

The best trained network using only G and T (the one with the smallest error) was selected and named MLP_{GT}. Also, the best trained network using G, T, AOI and K_T' was selected and denominated MLP_{ALL}. The performance of both models with respect to the *procedure 1* of IEC 60891 was also estimated. Herein the selected reference curve was the one acquired on 28 February 2011 at 13:16 under an irradiance $G = 1000$ W/m^2 and a module temperature $T = 30.2\,°\text{C}$. For the module used in this experiment, the values of the required intrinsic parameters are:

$$\alpha = 0.0027 \text{ A/°C}$$

$$\beta = 0.0706 \text{ V/°C}$$

$$\kappa = 0.0027 \,\Omega/°\text{C}$$

$$R_S = 0.264 \,\Omega$$

Taking into account the complete testing set (3056 samples not selected for the training phase), the MLP_{ALL} model obtains better results in terms of global relative error (1.9%) than the MLP_{GT} (2.1%) or the IEC_{60981} (3.8%) models. In Table 4 the mean relative curve errors of the three models for different irradiance ranges are summarised. As can be seen, the proposed method outperforms the other methods in all cases, although the greatest differences are obtained under high irradiance values.

Another criterion to compare the models is the percentage of examples of the testing set where the MLP_{ALL} model has less error than the other two models. From the results it can be stated that the

11

Irradiance (W/m^2)	IEC$_{60891}$	MLP$_{GT}$	MLP$_{ALL}$
200–400	8.4%	4.9%	4.8%
400–600	4.1%	3.3%	2.8%
600–800	3.0%	2.2%	1.8%
≥800	2.7%	1.0%	0.9%

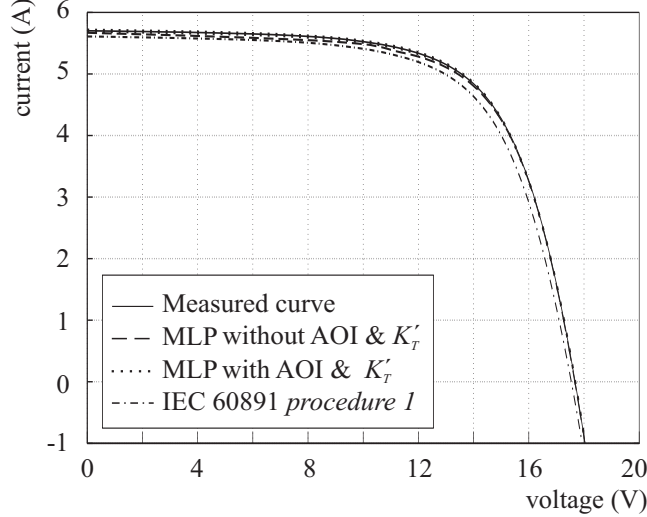Table 4: Relative curve error of the three models for different irradiance ranges.

Figure 7: Comparison of models for a curve measured on 24 March 2011.

MLP$_{ALL}$ model returns a better approximation (closer to the measured curve) than either the MLP$_{GT}$ or the IEC$_{60981}$ models over a total of 1609 examples (52.6%) whereas the MLP$_{GT}$ model performs best in only 1093 of the curves (35.8%). The IEC$_{60981}$ model outperforms the other two models over 354 examples only (11.6%).

In order to illustrate the performance of these models, several *I–V* curves amongst the testing set were selected. Fig. 7 is a typical example of an *I–V* curve acquired under a high irradiance value in which all models behave in a similar way. It was taken on 24 March 2011 at 12:01 with a global irradiance of 912 W/m^2 and a module temperature of $45.7\,°C$. The AOI was $23.8°$ and the normalised clearness index was 0.75. The visual difference between the true measured curve and each simulation is very small. It is necessary to zoom in to be able to see the difference between them (see Fig. 8). The curve provided by the MLP model using the angle of incidence and the normalised clearness index is closer to the measured curve than the ones obtained with the other models.

In many *I–V* curves the model trained with the angle of incidence and the normalised clearness gives better results than the model without those parameters. For instance, the *I–V* curve corresponding to 7 April 2011 at 10:21, with $G = 447$ W/m^2, $T = 28.6\,°C$, AOI = $57.7°$ and $K_T' = 0.69$ (see Fig. 9) is an example which confirms that the MLP$_{ALL}$ model performs better than the MLP$_{GT}$ and IEC$_{60981}$ models. In addition, the curve simulated by MLP$_{GT}$ has a odd behaviour (it does not emulate well the shape of the measured curve).

There are examples where none of the models gives a satisfactory approximation. For example, Fig. 10 shows an *I–V* curve measured on 28 February 2011 at 18:11 (with $G = 214$ W/m^2, $T = 18.7\,°C$, AOI = $74.9°$ and $K_T' = 0.84$). All the approximations are far from the measured curve being MLP$_{ALL}$ the best model. Again, the shape of the approximation given by the MLP$_{GT}$ model does not correspond to the typical shape of an *I–V* curve.
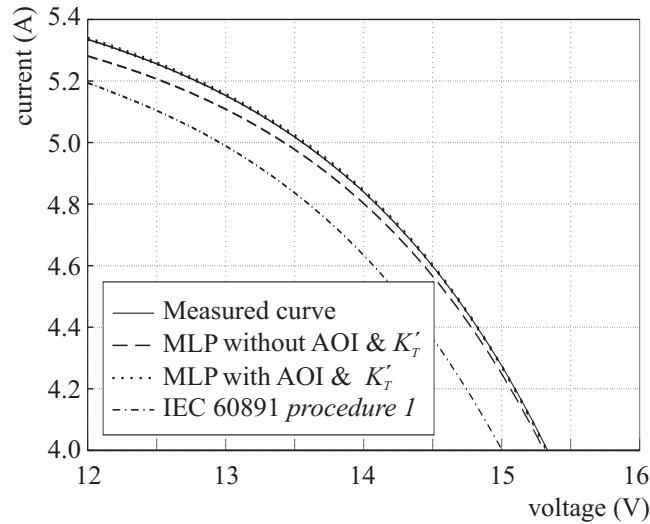
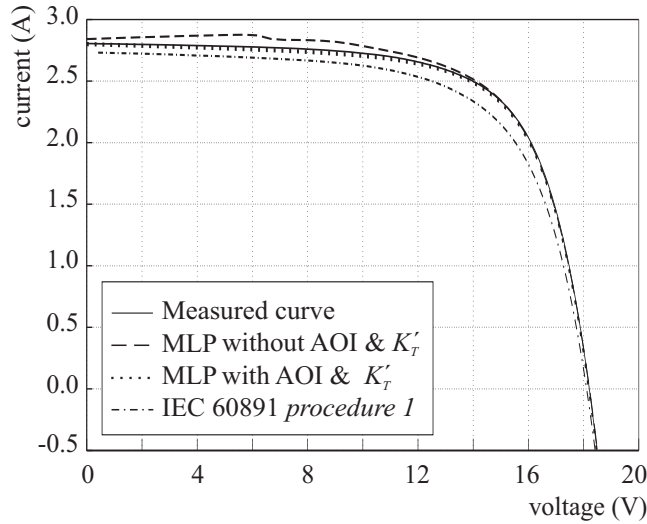Figure 8: Zoom in on the previous figure to see some difference.

Figure 9: Comparison of models for a curve measured on 7 April 2011.

6   Conclusions

In this paper, a new model to simulate *I–V* curves of photovoltaic modules is proposed. This model, based on the use of a multilayer perceptron neural network, can be used in combination with other models of the elements of a photovoltaic plant to predict its energy output. The main contribution with respect previous papers that already propose the use of neural networks is the incorporation of two new input variables: the angle of incidence and the normalised clearness index. The use of these new parameters allow to distinguish situations in which the solar irradiance and the module temperature are the same but the *I–V* curves are different.

The proposed model was compared to two previous models: the IEC 60891 method and a neural network model using only the irradiance and the module temperature. The obtained results prove that with the proposed model the error of the simulated *I–V* curve is less than 2%, being a significant improvement over the algebraic method, which duplicates this error.

A detailed curve-by-curve study was also performed over several examples amongst the testing set. In most of the cases the introduction of the angle of incidence and the instantaneous clearness index improves the results with respect to the other models. Moreover, the MLP trained only with G and T sometimes presents problems related to the shape of the curve. However, these problems
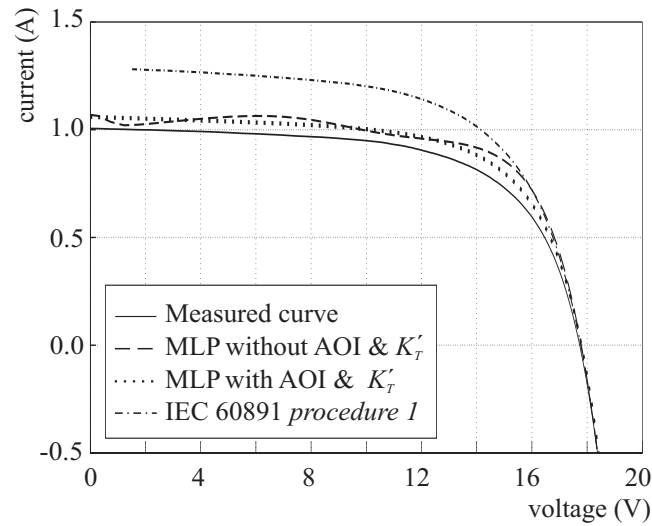
13

Figure 10: Comparison of models for a curve measured on 28 February 2011.

do not arise if the network is trained using the angle of incidence and the normalised instantaneous clearness index.

The proposed model allow us to improve the accuracy of tools used to forecast the energy output of photovoltaic plants. The methodology proposed in this work can be applied to other types of photovoltaic technologies including polycrystalline silicon, amorphous silicon and cadmium telluride.

Nomenclature

e Sun's topocentric elevation angle (°)

G Global irradiance on the module plane (W/m^2)

$G_{ext,b}$ Extraterrestrial global irradiance on a plane normal to the light beam (W/m^2)

G_{ext} Extraterrestrial global irradiance on an oriented surface (W/m^2)

I_{cutoff} Current of a cut–off point between two curves (A)

I_{M} Current at the maximum power point (A)

I_{SC} Short–circuit current of the module (A)

K_T Instantaneous clearness index

K_T' Normalised instantaneous clearness index

n Number of points of an I–V curve

P Atmospheric pressure (mbar)

P_0 Standard atmospheric pressure at sea level, constant (1013 mbar)

P_{M} Maximum power of the module (W)

R Sun–Earth distance (AU)

R_0 Mean Sun–Earth distance, constant (1 AU)

14

R_S Internal series resistance of the module (Ω)

S_0 Solar constant (1366.1 W/m^2)

T Module temperature (°C)

V_{cutoff} Voltage of a cut–off point between two curves (V)

V_M Voltage at the maximum power point (V)

V_OC Open–circuit voltage of the module (V)

α Module current temperature coefficient (A/°C)

β Module voltage temperature coefficient (V/°C)

Γ Sun's topocentric azimuth angle measured from the south, west positive (°)

γ Rotation angle of the module measured from the south, west positive (°)

κ Curve correction factor of the module (Ω/°C)

ω Slope or tilt angle of the module (°)

θ Sun's topocentric zenith angle (°)

AM Air mass factor

AM$_\mathrm{PC}$ Air mass factor corrected by pressure

ANN Artificial Neural Network

AOI Angle Of Incidence

IEC International Electrotechnical Commission

IEC$_{60891}$ *Procedure 1* of IEC 60891

MLP Multilayer Perceptron

MLP$_\mathrm{ALL}$ MLP trained with G, T, AOI and K'_T

MLP$_\mathrm{GT}$ MLP only trained with G and T

PV Photovoltaic

STC Standard Test Conditions

Acknowledgements

References

[1] IEC 60891. *Procedures for temperature and irradiance corrections to measure I–V characteristics of crystalline silicon photovoltaic devices*. International Electrotechnical Commission, Geneva (Switzerland), 2nd edition, 2009. ISBN 978-2-88910-316-4.

[2] G Blaesser and E Rossi. Extrapolation of outdoor measurements of PV array *I–V* characteristics to standard test conditions. *Solar Cells*, 25(2):91–96, 1988. doi: 10.1016/0379-6787(88)90014-2.

[3] AJ Anderson. Photovoltaic translation equations: A new approach. Technical Report NREL/TP-411-20279, National Renewable Energy Laboratory (NREL), Golden (CO, USA), 1996.

[4] B Marion. A method for modeling the current-voltage curve on a PV module for outdoor conditions. *Progress in Photovoltaics: Research and Applications*, 10(3):205–214, 2002. doi: 10.1002/pip.403.

[5] B Marion, S Rummel, and A Anderberg. Current-voltage curve translation by bilinear interpolation. *Progress in Photovoltaics: Research and Applications*, 12(8):593–607, 2004. doi: 10.1002/pip.551.

[6] E Karatepe, M Boztepe, and M Colak. Neural network based solar cell model. *Energy Conversion & Management*, 47(9–10):1159–1178, 2006. doi: 10.1016/j.enconman.2005.07.007.

[7] MC Di Piazza, M Pucci, A Ragusa, and G Vitale. Analytical versus neural Real-Time simulation of a photovoltaic generator based on a DC-DC converter. *IEEE Transactions on Industry Applications*, 46(10):2501–2510, 2010. doi: 10.1109/TIA.2010.2072975.

[8] JA Dolan, R Lee, YH Yeh, C Yeh, DY Nguyen, S Ben–Menahem, and AK Ishihara. Neural network estimation of photovoltaic *I–V* curves under partially shaded conditions. In *2011 International Joint Conference on Neural Networks (IJCNN)*, pages 1358–1365, 2011. doi: 10.1109/IJCNN.2011.6033382.

[9] F Almonacid, C Rus, L Hontoria, M Fuentes, and G Nofuentes. Characterisation of Si-crystalline PV modules by artificial neural networks. *Renewable Energy*, 34(4):941–949, 2009. doi: 10.1016/j.renene.2008.06.010.

[10] F Almonacid, C Rus, L Hontoria, and FJ Muñoz. Characterisation of PV CIS module by artificial neural networks A comparative study with other methods. *Renewable Energy*, 35(5):973–980, 2010. doi: 10.1016/j.renene.2009.11.018.

[11] LE Zárate, LVBM Neto, DA Soares, and FR Bittencout. Artificial neural networks applied for representation of curves Current-Voltage of photovoltaic modules. In *IEEE International Conference on Industrial Informatics*, pages 1644–1649, Daejeon (Korea), 2008. doi: 10.1109/INDIN.2008.4618367.

[12] F Bonanno, G Capizzi, G Graditi, C Napoli, and GM Tina. A radial basis function neural network based approach for the electrical characteristics estimation of a photovoltaic module. *Applied Energy*, 97:956–961, 2012. ISSN 0306-2619. doi: 10.1016/j.apenergy.2011.12.085.

[13] M Piliougine, D Elizondo, L Mora–López, and M Sidrach–de–Cardona. Photovoltaic module simulation by neural networks using solar spectral distribution. *Progress in Photovoltaics: Research and Applications*, Published online in May 2012. doi: 10.1002/pip.2209.

[14] SA Kalogirou. Applications of artificial neural-networks for energy systems. *Applied Energy*, 67(1-2):17–35, 2000. ISSN 0306-2619. doi: 10.1016/S0306-2619(00)00005-2.

[15] D Elizondo, G Hoogenboom, and RW McClendon. Development of a neural network model to predict daily solar radiation. *Agricultural and Forest Meteorology*, 71(1-2):115–132, 1994. doi: 10.1016/0168-1923(94)90103-1.

[16] J Soares, AP Oliveira, MZ Božnar, P Mlakar, JF Escobedo, and A J Machado. Modeling hourly diffuse solar-radiation in the city of São Paulo using a neural-network technique. *Applied Energy*, 79(2):201–214, 2004. ISSN 0306-2619. doi: 10.1016/j.apenergy.2003.11.004.

[17] A Yona, T Senjyu, AY Saber, T Funabashi, H Sekine, and CH Kim. Application of neural network to 24-hour-ahead generating power forecasting for PV system. In *IEEE Power and Energy Society General Meeting*, pages 1–6, Pittsburgh (PA, USA), 2008. doi: 10.1109/PES.2008.4596295.

[18] O Şenkal and T Kuleli. Estimation of solar radiation over Turkey using artificial neural network and satellite data. *Applied Energy*, 86(7–8):1222–1228, 2009. ISSN 0306-2619. doi: 10.1016/j.apenergy.2008.06.003.

[19] L Mora-López, M Piliougine, J Carretero, and M Sidrach-de-Cardona. Integration of statistical and machine learning models for short-term forecasting of the atmospheric clearness index. In *5th Biennial Meeting of International Congress on Environmental Modelling and Software (iEMSs)*, Ottawa (Canada), 2010.

[20] L Zhang and YF Bai. On-line neural network training for maximum power point tracking of PV power plant. *Transactions of the Institute of Measurement and Control*, 30(1):77–96, 2008. doi: 10.1177/0142331207076374.

[21] KH Chao, CJ Li, and MH Wang. A maximum power point tracking method based on extension neural network for PV systems. In *6th International Symposium on Neural Networks on Advances in Neural Networks*, volume 1, pages 745–755, Wuhan (China), 2009. doi: {10.1007/978-3-642-01507-6_84}.

[22] I Reda and A Andreas. Solar position algorithm for solar radiation applications. Technical Report NREL/TP-560-34302, National Renewable Energy Laboratory (NREL), Golden (CO, USA), 2008.

[23] CA Gueymard. The Sun's total and spectral irradiance for solar energy applications and solar radiation models. *Solar Energy*, 76(4):423–453, 2004. doi: 10.1016/j.solener.2003.08.039.

[24] F Kasten and A Young. Revised optical air mass tables and approximation formula. *Applied Optics*, 28(22):4735–4738, 1989. doi: 10.1364/AO.28.004735.

[25] RE Bird and C Riordan. Simple solar spectral model for direct and diffuse irradiance on horizontal and tilted planes at the Earth's surface for cloudless atmospheres. *Journal of Climate and Applied Meteorology*, 25(1):87–97, 1986. doi: 10.1175/1520-0450(1986)025$\langle$0087: SSSMFD$\rangle$2.0.CO;2.

[26] A Woyte, R Belmans, and J Nijs. Fluctuations in instantaneous clearness index: Analysis and statistics. *Solar Energy*, 81(2):195–206, 2007. doi: 10.1016/j.solener.2006.03.001.

[27] R Pérez, P Ineichen, R Seals, and A Zelenka. Making full use of the clearness index for parameterizing hourly insolation conditions. *Solar Energy*, 45(2):111–114, 1990. doi: 10.1016/0038-092X(90)90036-C.

[28] M Piliougine, J Carretero, L Mora-López, and M Sidrach-de-Cardona. Experimental system for current-voltage curve measurement of photovoltaic modules under outdoor conditions. *Progress in Photovoltaics: Research and Applications*, 19(5):591–602, 2011. doi: 10.1002/pip.1073.

[29] JC Principe, JR Euliano, and WC Lefebvre. *Neural and Adaptive Systems: Fundamentals through Simulations*. John Wiley & Sons, New York (NY, USA), 2000. ISBN 978-0-471-35167-2.